Lifetime measurements in the chiral-candidate doublet bands of ^{130}La

M. Ionescu-Bujor,[1] S. Aydin,[2] N. Mărginean,[1] C. Costache,[1] D. Bucurescu,[1] N. Florea,[1] T. Glodariu,[1,*] A. Ionescu,[1,3] A. Iordăchescu,[1] R. Mărginean,[1] C. Mihai,[1] R. E. Mihai,[1] A. Mitu,[1] A. Negreţ,[1] C. R. Niţă,[1] A. Olăcel,[1] S. Pascu,[1] B. Saygi,[4] L. Stroe,[1] R. Suvăilă,[1] S. Toma,[1] and A. Turturică[1]

[1]*Horia Hulubei National Institute of Physics and Nuclear Engineering, 077125 Bucharest-Măgurele, Romania*

[2]*Department of Physics, Aksaray University, 68100 Aksaray, Turkey*

[3]*Faculty of Physics, University of Bucharest, 077125 Bucharest-Măgurele, Romania*

[4]*Department of Physics, Faculty of Science, Ege University, Bornova, 35100 Izmir, Turkey*

(Received 2 August 2018; published 20 November 2018)

The lifetimes of the excited states belonging to the chiral-candidate doublet bands built on the $\pi h_{11/2} \otimes \nu h_{11/2}^{-1}$ configuration in ^{130}La have been measured by applying the Doppler-shift attenuation method and the in-beam fast timing technique. Excited states were populated in the ^{121}Sb(^{12}C, $3n$) reaction at a bombarding energy of 54 MeV. The 7^+ bandhead of the yrast band was identified as an isomeric state with a lifetime of $\tau(7^+) = 0.38(7)$ ns. Similar reduced transition probabilities $B(M1)$ and $B(E2)$ were found for the states with the same spin in the partner bands. The results revealed an even-odd spin dependence in the $B(E2)$ values, whereas the $B(M1)$ values vary nearly monotonically with increasing spin. The experimental properties of the doublet bands in ^{130}La are compared with theoretical calculations done in the frame of the two-quasiparticles-plus-triaxial-rotor model. The static chirality is not supported by the obtained data; however, chiral vibrations cannot be excluded.

DOI: 10.1103/PhysRevC.98.054305

I. INTRODUCTION

Considerable experimental and theoretical effort was invested in the last two decades for unambiguous identification of chirality in rotating nuclei. Nuclear chirality is generated when the total angular momentum vector of a triaxial nucleus is out of the three symmetry planes of the triaxial mean field [1,2]. This situation can occur when the proton and neutron Fermi levels are located in the lower part of the valence proton high-j (particle-like) and in the upper part of the valence neutron high-j (hole-like) subshells (or vice versa). The chiral motion evolves from chiral vibration at low spins to chiral rotation at high spins, which corresponds to static chirality. The experimental manifestation of the intrinsic chirality is a structure of two, almost degenerate, $\Delta J = 1$ rotational bands having equal parity and linked to each other by interband γ-ray transitions. Chiral-candidate bands were first reported in odd-odd nuclei of the $A \approx 130$ mass region, where side band partners of the yrast bands built on the $\pi h_{11/2} \otimes \nu h_{11/2}^{-1}$ configuration were identified [3,4]. Since then, about 60 chiral doublet bands have been discovered in nuclei with $A \approx 80$, 100, 130, and 190, including odd-odd, odd-A, and even-even nuclei [5]. Theoretically, the chiral doublet bands have been investigated in the frameworks of the particle rotor model [1,6–11], the tilted axis cranking (TAC) model [1,2,12,13], the TAC plus random-phase approximation [14], and the core-particle-hole coupling model [15]. Descriptions of the doublet bands were also provided within the interacting boson-fermion-fermion model [16,17] and the angular momentum projection approach [18–20].

The fingerprints for static chirality have been specified by several theoretical calculations [6,7,15]. Apart from the observation of nearly degenerate bands, there are selection rules for the electromagnetic transitions in the chiral geometry. The reduced transition strengths, $B(E2)$ and $B(M1)$, for the in-band transitions should be comparable for both the bands. Furthermore the reduced transition probability ratios $B(M1)/B(E2)$ as well as the $B(M1)$ values should exhibit odd-even staggering.

Electromagnetic transition probabilities have been measured to establish chirality in several odd-odd nuclei of the $A \approx 130$ mass region, i.e., ^{124,126,128,130}Cs [21–25], ^{132}La [23], and ^{134}Pr [26]. Similar $B(E2)$ and $B(M1)$ values in the side and the yrast bands, as well as characteristic staggering of reduced $M1$ transition probabilities inside bands, were reported first in ^{128}Cs [23], leading to the identification of this nucleus as potentially the best case revealing chiral geometry in odd-odd nuclei. Subsequent lifetime measurements carried out in ^{124}Cs [21,22], ^{126}Cs [24], and ^{130}Cs [25] also gave support to the chiral interpretation. On the other hand, lifetime experiments in ^{132}La [23] and ^{134}Pr [26] demonstrated that the $B(E2)$ values in the chiral-candidate doublet bands differ considerably from each other, and moreover no staggering is seen in $B(M1)$ values. Thus, for these nuclei the chiral scenario does not seem to hold.

In the present work the chirality phenomenon is studied in the odd-odd ^{130}La nucleus via lifetime measurements of the excited states. ^{130}La is one the first nuclei in which a side band partner of the yrast band was observed [4]. In our experiment the lifetimes of the high-spin states in the yrast

*Deceased.

and side band were investigated by applying the Doppler-shift attenuation method (DSAM). Information about the lifetimes of the lowest-lying states of the yrast band were obtained by using the in-beam fast timing method. In the performed study the high-spin level scheme of ^{130}La was substantially extended. New band structures were identified and level lifetimes were measured. The results of the detailed spectroscopic investigation will be published in a forthcoming paper [27].

II. EXPERIMENTAL PROCEDURE

Excited states in ^{130}La were populated using the reaction ^{121}Sb(^{12}C, $3n$) at a bombarding energy of 54 MeV. The beam was provided by the FN Tandem accelerator of the Horia Hulubei National Institute of Physics and Nuclear Engineering (IFIN-HH) in Bucharest. The target consisted of a 1 mg/cm^2 isotopically enriched ^{121}Sb layer evaporated on a 50 mg/cm^2 ^{208}Pb foil, in which both the reaction products and the beam were stopped. The γ transitions of ^{130}La were measured using the ROSPHERE mixed array [28], consisting of 14 high-purity germanium (HPGe) detectors and 11 $LaBr_3$(Ce) scintillator detectors. The HPGe detectors were placed in three rings at the angles of 143°, 90°, and 37° with respect to the beam axis. The $LaBr_3$(Ce) scintillators were placed in angular rings at 110°, 90°, and 70° with respect to the beam direction. Data were recorded by requesting either a threefold coincidence, namely that γ rays were observed in $\geqslant$2 $LaBr_3$(Ce) detectors and $\geqslant$1 HPGe detector, or a twofold HPGe-HPGe coincidence. The energy calibration was done using a ^{152}Eu source, which also was used to determine the energy-dependent time walk of the experimental setup. The data from the HPGe detectors were sorted into a symmetric γ-γ matrix and three asymmetric matrices having the detectors in each ring on the first axis and all detectors on the second axis. The γ-ray intensities were derived from spectra created using the symmetric matrix, while the asymmetric matrices were used for DSAM analyses.

In fast-timing measurements, lifetimes of excited states were extracted from the time difference between two γ rays observed in pairs of $LaBr_3$(Ce) detectors. The instrument time response for each $LaBr_3$(Ce) detector and constant fraction discriminator (CFD) combination in the array required an offline correction because of time walk. To achieve this, the method described by Mărginean *et al.* in Ref. [29] was used. After correcting for the time walk, data were sorted into $E_{\gamma 1}$-$E_{\gamma 2}$-ΔT cubes, where $E_{\gamma 1}$ and $E_{\gamma 2}$ represent the energy measured in the $LaBr_3$(Ce) detectors. To further clean the cascade of interest detected in the $LaBr_3$(Ce) detectors, additional γ rays detected in the HPGe were used as a gate.

III. EXPERIMENTAL RESULTS

A partial level scheme of ^{130}La showing the chiral candidate bands built on the $\pi h_{11/2} \otimes \nu h^{-1}_{11/2}$ configuration is illustrated in Fig. 1. The previously reported yrast band [30,31] was observed in the present experiment up to spin $J = 20$. Firm spin and parity assignments for this band were established in our recent study [32], in which the yrast bandhead decay to the ground state was elucidated. The side band proposed in Ref. [4] was confirmed by the present measurements. Five new transitions, with energies of 343.4, 385.2, 492.3, 863.0, and 877.5 keV, were included in this band, which was extended by two more states, with spins 17^+ and 18^+. The 11^+ state of the side band was linked with the 9^+ state of the yrast band by a new transition of 692.3 keV. A weak transition of 179.3 keV was included between the 10^+ and 8^+ states of the yrast band. Two new transitions of 128.7 and 137.6 keV were found to deexcite the 7^+ and 8^+ states, respectively, feeding the previously identified 7^- state at 488.8 keV [32], while a transition of 292.7 keV was placed between the 7^+ state and a new 6^- state at 324.8 keV excitation energy [27]. The γ intensities of the transitions in the partner bands have been derived. Moreover information about transition multipolarities were obtained from measured angular distribution ratios using spectra from asymmetric matrices. For the in-band transitions with $\Delta J = 1$, it was found that they have $M1$ character with a negligible $E2$ component. The data for the 740.4-, 841.2-, and 766.4-keV interband transitions indicated a mixed $M1 + E2$ character; however, the statistics was not enough to derive the mixing ratios. Detailed spectroscopic results obtained in this experiment will be given in a subsequent paper [27].

A. Lifetime measurements with Doppler shift attenuation method

By applying the Doppler-shift attenuation method, lifetimes of the levels with $J^\pi = 13^+$ to 20^+ in the yrast band and with $J^\pi = 14^+$ to 18^+ in the side band have been derived. To obtain the line line shapes of the investigated γ-ray transitions, gates were set in the γ-γ coincidence matrices on appropriate lower-lying transitions emitted from stopped nuclei. The analysis was performed using the LINESHAPE computer code [33]. The slowing-down history of ^{130}La recoils in the target and backing was simulated using Monte Carlo techniques and a statistical distribution was created for the projection of the recoil velocity with respect to the direction of the detected γ ray. Moreover, the kinematic effects of the nucleon evaporation were included, as well as the finite solid angle of the detectors. For the description of the electronic and nuclear scattering, the Ziegler stopping powers [34,35] were used. Extraction of lifetimes was done step by step, starting from the upper levels. The intensities of the γ rays involved in the analysis were derived from the symmetric γ-γ matrix. Due to the presence of Doppler-broadened shapes, the γ intensities were obtained by integrating on the broadened lines. At each level the intensity balance of feeding and decaying transitions was investigated, allowing us to establish the amount of side-feeding from unobserved transitions. Effective side-feeding times dependent on the level spin were used according to the procedure developed in [36].

For all investigated states, line-shape analysis was performed for the $E2$ deexciting transitions, except for the 14^+ state of the side band, where the 740-keV $M1$ transition to the 13^+ state of the yrast band was analyzed. For the 15^+ and 16^+ states of the yrast band and the 15^+ state of the side band, line shapes of the in-band $M1$ transitions were also analyzed. In these cases the adopted lifetimes were obtained as an average of the values derived in the two independent analyses.

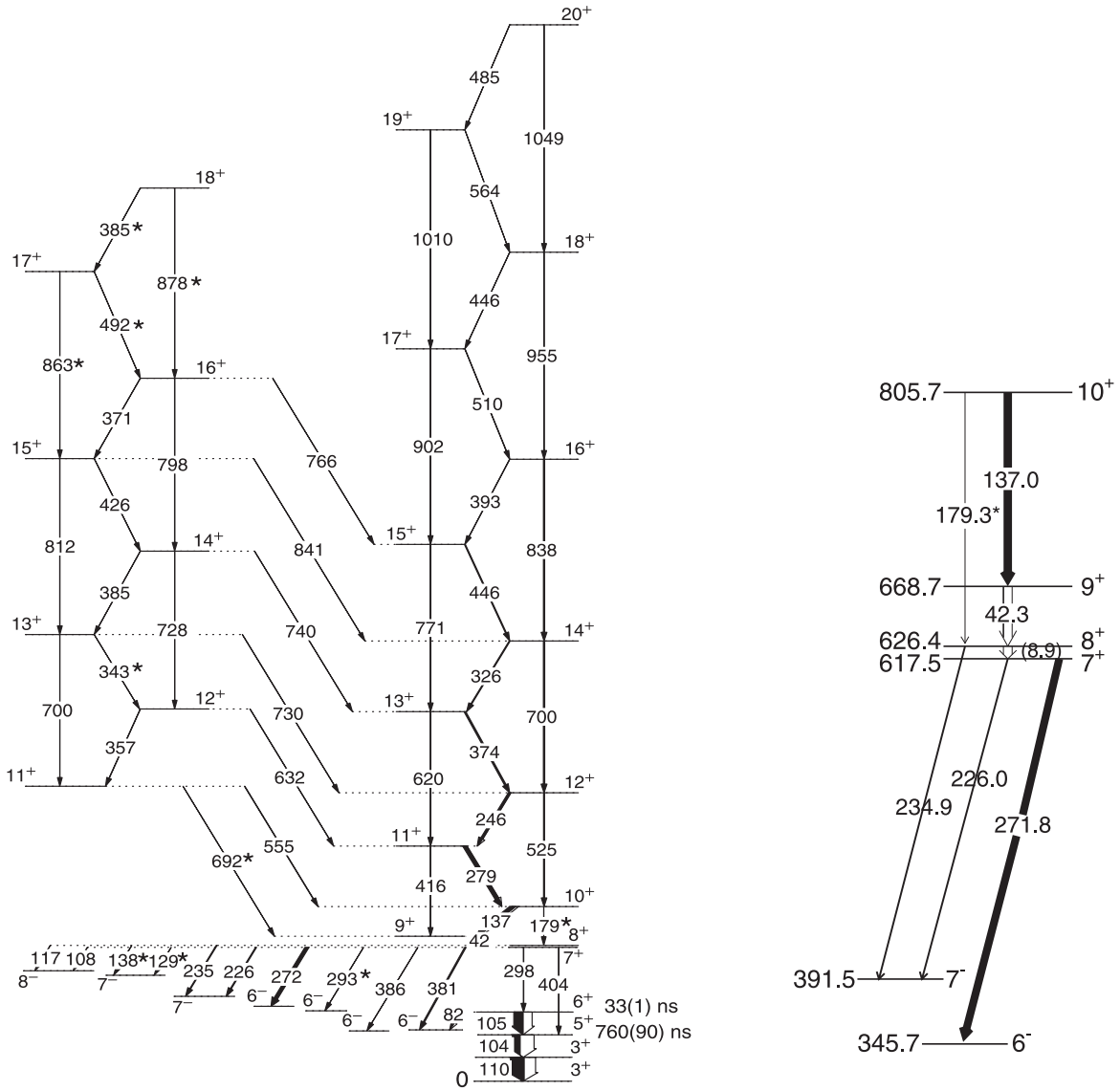

FIG. 1. Left: Partial level scheme of ^{130}La showing the yrast and the side bands of the $\pi h_{11/2} \otimes \nu h^{-1}_{11/2}$ configuration, as well as the decay out of the yrast band, from Refs. [4,30–32] and present work. New transitions observed in the present work are marked with a star. The widths of the arrows represent the relative intensity of the γ-ray transitions (from Ref. [32] and present experiment), with the internal conversion contribution indicated by the white component of the arrow. Energies are given in keV. Right: Expanded view of the lower part of the yrast band and the most intense transitions of its decay.

Examples of experimental line shapes and the corresponding fits are illustrated in Figs. 2 and 3. The derived lifetimes are collected in Table I. Assigned errors include the uncertainties due to the stopping power calculation (10%) and to the side-feeding pattern (15%).

B. Lifetime measurements with fast-timing technique

The lifetimes of the lowest lying states of the yrast band were investigated by using the fast-timing technique. For this purpose, feeding and deexciting transitions were selected for the levels of interest, and corresponding time difference spectra were created. To clean the coincidence spectra, appropriate gates were put in the HPGe spectra. In the present case the time resolution was larger than the lifetimes being measured, therefore the centroid method was used [29]. Two time distributions were obtained by gating on the two transitions as start and stop in both possible ways. The time difference ΔC between the centroid positions of the two decay distributions is twice the lifetime τ. Illustrative energy spectra obtained with HPGe and $LaBr_3$(Ce) are presented in Fig. 4. Figure 5 shows the time-difference spectra obtained by gating on the discrete feeding and de-exciting transitions across levels of interest in the sorted $E_{\gamma 1}$-$E_{\gamma 2}$-ΔT cubes, with additional conditions set in the HPGe detectors.

To derive the lifetime of the 10^+ member of the yrast band, the 279–137-keV γ-ray cascade feeding and deexciting the state was investigated. As illustrated in Figs. 1 and 4, an intense transition of 272 keV is present in the decay of the yrast band. The 272- and 279-keV γ lines are not separated

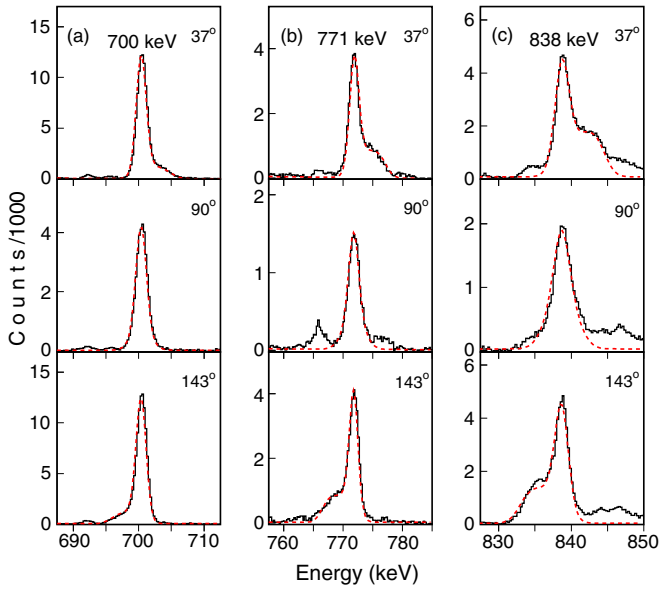

FIG. 2. Experimental and calculated lineshapes for transitions deexciting the states in the yrast band of ^{130}La with $J^\pi = 14^+$ (a), 15^+ (b), and 16^+ (c). The coincidence spectra were created with narrow gates on lower-lying transitions emitted from stopped nuclei. The fitted DSAM spectra are shown in red dashed lines.

in the spectra registered with the $LaBr_3$(Ce) detectors. To avoid contamination from the coincidences with the 272-keV transition, a gate was put on this transition in the HPGe spectrum. Delayed coincidence time spectra obtained using as start the 279-keV transition and as stop the 137-keV one

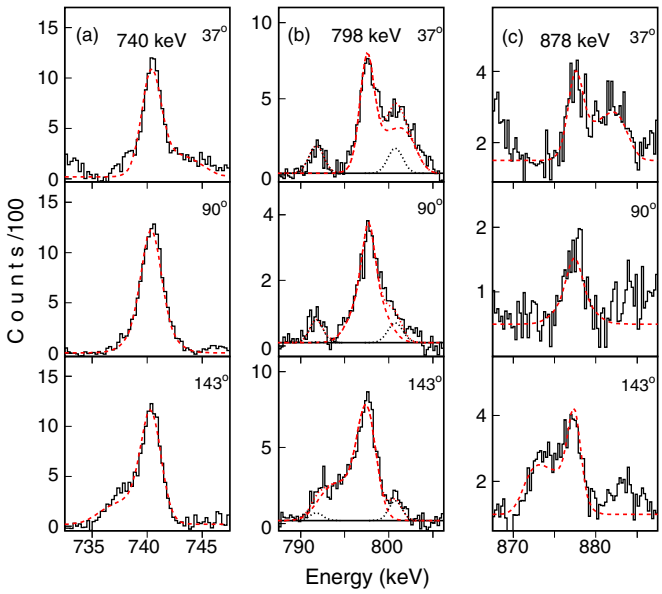

FIG. 3. Experimental and calculated lineshapes for transitions deexciting the states in the side band of ^{130}La with $J^\pi = 14^+$ (a), 16^+ (b), and 18^+ (c). The coincidence spectra were created with narrow gates on lower-lying transitions emitted from stopped nuclei. Contaminant peaks are shown in dotted lines and the fitted DSAM spectra in red dashed lines.

TABLE I. Lifetimes determined in the present work by DSAM for excited states belonging to the yrast and side bands built on the $\pi h_{11/2} \otimes \nu h_{11/2}^{-1}$ configuration in ^{130}La.

E_x (keV)	J^π	τ (ps)
yrast band		
1705.0	13^+	1.73(38)
2031.0	14^+	1.17(21)
2476.5	15^+	0.87(17)
2869.3	16^+	0.60(11)
3378.7	17^+	0.46(10)
3824.4	18^+	0.41(10)
4388.9	19^+	0.60(13)
4873.5	20^+	0.55(12)
side band		
2445.4	14^+	0.41(12)
2872.3	15^+	0.53(13)
3243.0	16^+	0.50(13)
3735.3	17^+	0.59(13)
4120.5	18^+	0.61(13)

(black), and as start the 137-keV transition and as stop the 279-keV one (red), are shown in Fig. 5(a). No shift in the centroid position of the two time spectra was observed. Based on the accumulated statistics and the resolution of the time spectra, we estimated that a lifetime of around 30 ps would have been observable. We therefore assigned an upper limit of $\tau < 30$ ps for the 10^+ state.

The 9^+ state is deexcited by a low-energy transition of 42.3 keV, that is below the energy threshold of the present experimental setup. The 8^+ state decays mainly by an unobserved transition of 8.9 keV feeding the 7^+ bandhead [32], as well as by three $E1$ transitions of 116.9, 137.6, and 234.9 keV, towards negative parity states. To derive the lifetime, we investigated the coincidence between the 137-keV transition from the 10^+ state and the 235-keV transition, the strongest $E1$ transition observed in the decay of the 8^+ state. As seen in Fig. 4(d), the 235-keV transition is masked by the intense transition of 246 keV between the 12^+ and 11^+ states of the yrast band. To clean the $LaBr_3$(Ce) spectra and to avoid contamination with the coincidence of the 246- and 137-keV γ rays, a gate was put in HPGe on the 246-keV line. The obtained spectrum [Fig. 4(c)] contains, however, besides the 235-keV transition, the γ-line of 226 keV deexciting the 7^+ state with a longer lifetime (see below). In order to avoid the contribution of this transition, a narrow gate was put on the right half of the 235-keV peak. The delayed coincidence time spectra corresponding to the pair of 137–235-keV γ-ray transitions, obtained by gating on the two transitions as start and stop in both possible ways, are shown in Fig. 5(b). A clear shift ΔC of the centroid positions was observed. Note that this shift is due to the lifetime of the 8^+ state, as well as that of the 9^+ intermediate level (Fig. 1, left). Based on systematics and theoretical considerations (see below), it is expected that the lifetime of the 9^+ state is much shorter than that of the 8^+ state. On the basis of the observed shift, we derived a lifetime $\tau = 120^{+20}_{-40}$ ps for the 8^+ state, with the assigned asymmetric

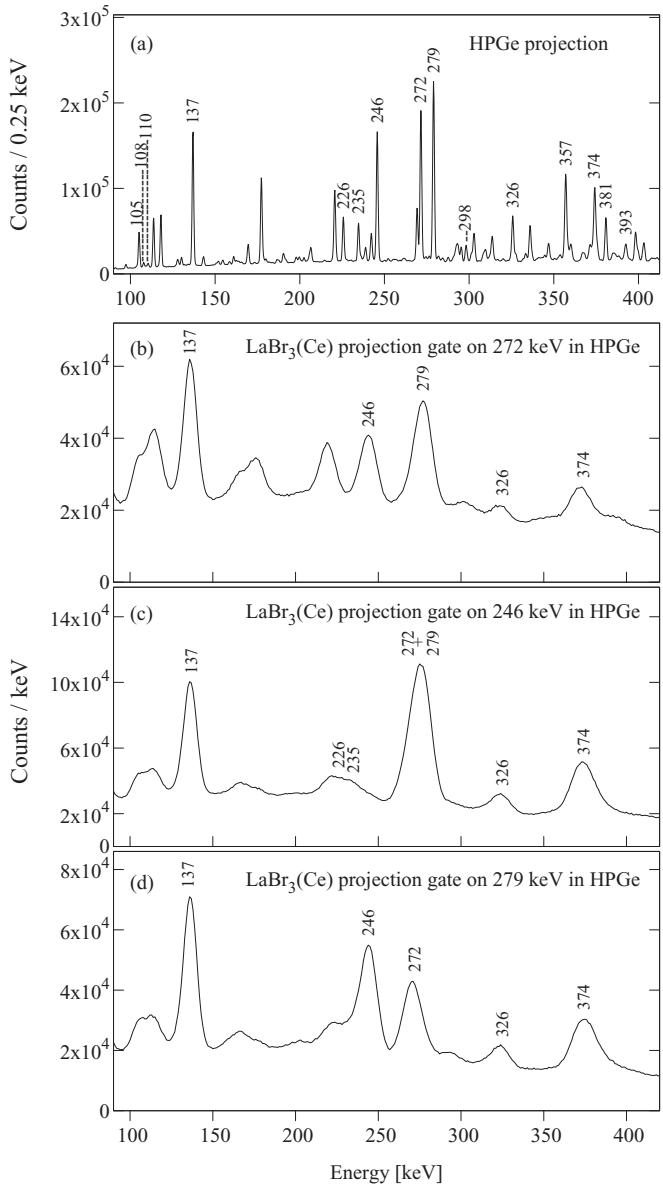

FIG. 4. (a) Energy projection of the γ-γ coincidence HPGe matrix in the energy range from 100 to 400 keV. The transitions belonging to the yrast band and its decay are labeled by energy. (b)–(d) γ-ray spectra from the $LaBr_3$(Ce) detectors with gates on selected transitions in the HPGe detectors.

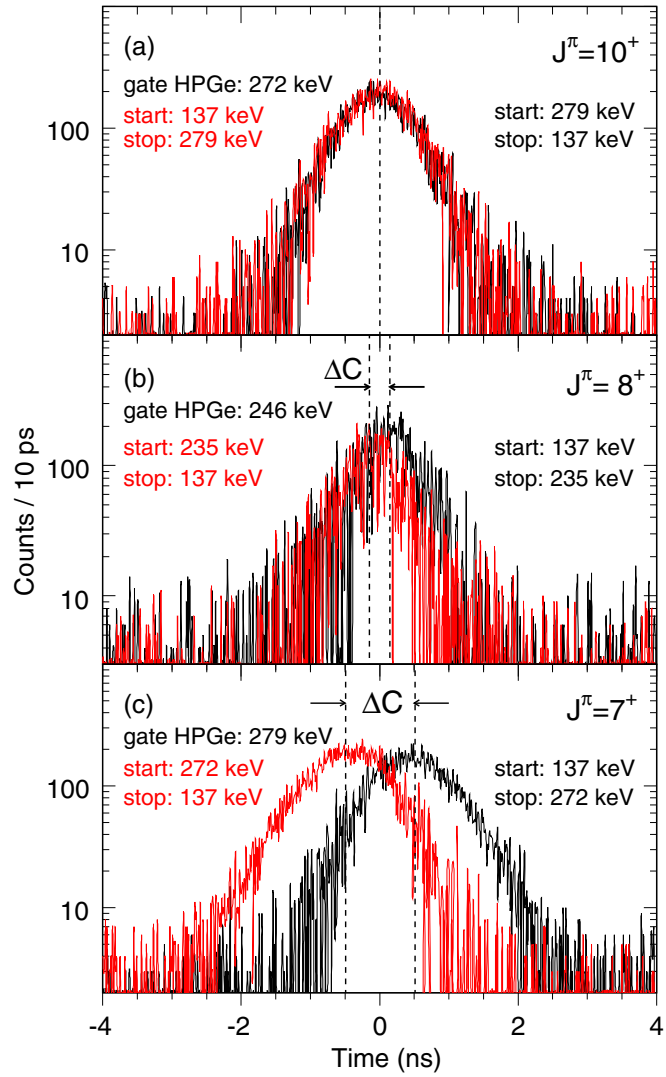

FIG. 5. Time difference spectra obtained from the $LaBr_3$(Ce) $E_{\gamma 1}$-$E_{\gamma 2}$-ΔT cube for selected pair of transitions in ^{130}La. Additional gates were put on appropriate γ rays in the HPGe detectors.

error including the possible contribution from the lifetime of the 9^+ state.

The 7^+ state, the lowest member of the structure built on the $\pi h_{11/2} \otimes \nu h_{11/2}^{-1}$ configuration, has a complex decay involving nine transitions, with the 272-keV transition being the most intense one (see Fig. 1). To derive the lifetime of the level, delayed coincidences between the 137-keV γ ray from the 10^+ state and the 272-keV γ-ray deexciting transition were investigated. In this case the gate in the HPGe detectors was put on the 279-keV γ ray from the yrast band. Figure 5(c) illustrates the shift of the centroids in the time spectra corresponding to the pair of 137–272-keV γ-ray transitions, obtained by gating on the two transitions as start and stop in both possible ways. The lifetime of the 7^+ state was also derived by investigating the coincidence between the 137- and 226-keV transitions, using a thin gate on the left half of the 226-keV peak in spectra obtained by gating on the 246-keV line in the HPGe detectors [see Fig. 4(c)]. The two independent analyses provided similar values for the shift of the centroid positions in the corresponding time spectra. Using the deduced centroid shift, corrected for the contribution due to the 9^+ and 8^+ intermediate states, a lifetime of $\tau = 380(70)$ ps was established for the 7^+ state. The results of the lifetime measurements using the fast-timing technique are collected in Table II.

IV. DISCUSSION

Experimental reduced transition probabilities derived on the basis of the lifetimes and γ intensities determined in the present work are given in Table III. The in-band and interband $\Delta J = 1$ transitions were assumed to be of pure

TABLE II. Lifetimes of the lowest states of the yrast band in ^{130}La determined in the present work by fast timing method.

E_x (keV)	J^π	τ (ns)
617.5	7^+	0.38(7)
626.4	8^+	$0.12^{+0.02}_{-0.04}$
805.7	10^+	<0.03

$M1$ type according to angular distribution data of the present experiment.

With its quite high lifetime value of 0.38(7) ns, the 7^+ state, the lowest member of the $\pi h_{11/2} \otimes \nu h^{-1}_{11/2}$ configuration, can be called an isomeric state. As seen in Table III, the 7^+ state decays via seven $E1$ transitions to negative-parity states of spin 6^-, 7^-, or 8^-. These transitions correspond to configuration changes from $\pi h_{11/2} \otimes \nu h^{-1}_{11/2}$ for the initial state into $\pi(d_{5/2}g_{7/2}) \otimes \nu h^{-1}_{11/2}$ or $\pi h_{11/2} \otimes \nu(d_{5/2}g_{7/2}d_{3/2}s_{1/2})$ for the final state. The $\pi h_{11/2} \to \pi(d_{5/2}g_{7/2})$ or $\nu h_{11/2} \to \nu(d_{5/2}g_{7/2}d_{3/2}s_{1/2})$ $E1$ transitions are forbidden in spherical nuclei by the selection rules for the $E1$ operator. However, in deformed nuclei small admixtures of the $f_{7/2}$ and $h_{9/2}$ orbitals into the negative-parity odd-nucleon wave function and of the $g_{9/2}$ orbital into the positive-parity odd-nucleon wave function allow for $E1$ transitions. Since these admixture are small, the corresponding $E1$ matrix elements are also small, which explains the large observed hindrances. The 7^+ state decays also toward the 5^+ and 6^+ low-lying positive-parity states, through the $E2$ 403.5- and $M1$ 298.4-keV hindered transitions, respectively (see Fig. 1 and Table III). The structure of the 5^+ and 6^+ isomeric states was discussed in Ref. [32], and involves the coupling of proton and neutron located in the deformed gds orbitals of the $N = 4$ shell. To explain the observed transitions from the 7^+ bandhead, small $\pi h_{11/2} \otimes \nu h_{11/2}$ components have to be present in the wave functions of the positive-parity states. It is worthwhile to mention that a 7^+ isomeric bandhead for the yrast band of the $\pi h_{11/2} \otimes \nu h^{-1}_{11/2}$ configuration has been reported in neighbor odd-odd nuclei ^{134}Pr ($\tau = 4.6(1)$ ns [38]) and ^{132}La ($\tau = 0.23(2)$ ns, weighted average of the values reported in [39]). Their decay also involves strongly hindered $E1$ transitions; e.g., by using the γ-intensities reported in [40] we deduced $B(E1)(82.4\text{ keV}) = 5.7(2.3) \times 10^{-7}$ W.u. and $B(E1)(306.6\text{ keV}) = 2.77(15) \times 10^{-6}$ W.u. for the transitions deexciting the 7^+ state in ^{134}Pr.

The 8^+ state, the first excited member of the $\pi h_{11/2} \otimes \nu h^{-1}_{11/2}$ configuration, decays mainly to the 7^+ bandhead via the highly converted 8.9-keV transition, with a total conversion coefficient $\alpha_{\text{tot}} = 198(3)$ [37]. A large reduced transition probability, $B(M1)(8.9\text{ keV}) = 1.58^{+0.98}_{-0.86}$ W.u., was derived for it. For the 137.0-keV transition deexciting the 10^+ state a lower limit $B(M1)(137.0\text{ keV}) > 0.28$ W.u. was established. Recently the lifetimes of the 8^+ and 10^+ members of the $\pi h_{11/2} \otimes \nu h^{-1}_{11/2}$ band in ^{132}La were reported as $\tau(8^+) = 104(8)$ ps and $\tau(10^+) = 3.0(4)$ ps [39]. Using the intensities given in [41] for the involved transitions, large reduced transition probabilities are derived, i.e., $B(M1)(38.1\text{ keV}, 8^+ \to 7^+) = 1.37(15)$ W.u. and $B(M1)(160.7\text{ keV}, 10^+ \to 9^+) = 1.98(26)$ W.u. On the basis of these results, it should be expected that also the 9^+ band member decays via an enhanced $M1$ transition. Assuming a transition strength of 1.5 W.u. for

TABLE III. Reduced transition probability values derived using the lifetimes reported in Tables I and II and total conversion coefficients taken from Ref. [37]. Relative γ intensities I^{rel}_γ are from Ref. [32] and the present experiment. Reduced transition probabilities are given in Weissskopf units.

E_i (keV)	J^π_i	J^π_f	E_γ (keV)	I^{rel}_γ	$B(E1) \times 10^{-6}$ (W.u.)	$B(M1)$ (W.u.)	$B(E2)$ (W.u.)
yrast							
617.5	7^+	8^-	108.0(2)	1.8(3)	26.8(6.8)		
		7^-	128.7(3)	0.7(2)	6.1(2.2)		
		7^-	226.0(2)	6.6(5)	10.7(2.1)		
		6^-	271.8(2)	25.2(13)	23.5(4.6)		
		6^-	292.7(2)	1.8(4)	1.3(4)		
		6^+	298.4(2)	2.9(11)		0.00017(7)	
		6^-	380.9(2)	9.5(11)	3.2(7)		
		6^-	385.5(2)	0.60(24)	0.2(1)		
		5^+	403.5(2)	3.3(9)			0.3(1)
626.4	8^+	7^+	8.9(2)	0.20(8)		$1.58^{+0.98}_{-0.86}$	
		8^-	116.9(2)	0.20(8)	$8.4^{+5.2}_{-4.6}$		
		7^-	137.6(3)	1.0(3)	$25.6^{+14.3}_{-12.3}$		
		7^-	234.9(2)	6.2(6)	$32.1^{+15.5}_{-12.4}$		
805.7	10^+	9^+	137.0(2)	27.4(14)		>0.28	
		8^+	179.3(3)	0.5(2)			>46
1705.0	13^+	12^+	374.3(2)	11.3(22)		0.24(8)	
		11^+	620.2(3)	4.5(12)			36(14)
2031.0	14^+	13^+	326.0(2)	6.4(19)		0.31(12)	
		12^+	700.3(2)	9.4(23)			62(22)
2476.5	15^+	14^+	445.5(3)	6.4(17)		0.24(9)	
		13^+	771.4(4)	4.6(11)			36(13)
2869.3	16^+	15^+	392.8(2)	2.7(8)		0.20(8)	
		14^+	838.3(5)	8.8(22)			63(23)
3378.7	17^+	16^+	509.6(6)	2.7(7)		0.23(9)	
		15^+	902.2(6)	3.3(7)			41(14)
3824.4	18^+	17^+	445.7(7)	0.9(3)		0.17(8)	
		16^+	955.1(6)	3.9(7)			52(18)
4388.9	19^+	18^+	564.4(6)	0.5(2)		0.07(4)	
		17^+	1010.2(8)	1.6(4)			24(10)
4873.5	20^+	19^+	484.6(8)	0.5(2)		0.08(4)	
		18^+	1049.1(8)	2.4(7)			25(11)
side							
2445.4	14^+	13^+	384.8(3)	1.13(17)		0.54(19)	
		12^+	728.1(6)	0.63(14)			55(21)
		13^+	740.4(3)	1.08(25)		0.073(29)	
2872.3	15^+	14^+	426.4(4)	1.36(31)		0.30(11)	
		13^+	811.7(6)	1.72(22)			56(17)
		14^+	841.3(9)	0.36(14)		0.010(5)	
3243.0	16^+	15^+	370.7(9)	0.90(21)		0.33(12)	
		15^+	766.4(7)	0.57(18)		0.024(10)	
		14^+	797.6(5)	1.83(20)			71(21)
3735.3	17^+	16^+	492.3(6)	0.82(18)		0.20(7)	
		15^+	863.0(6)	1.08(24)			40(14)
4120.5	18^+	17^+	385.2(8)	0.18(7)		0.10(5)	
		16^+	877.5(8)	1.48(18)			59(16)

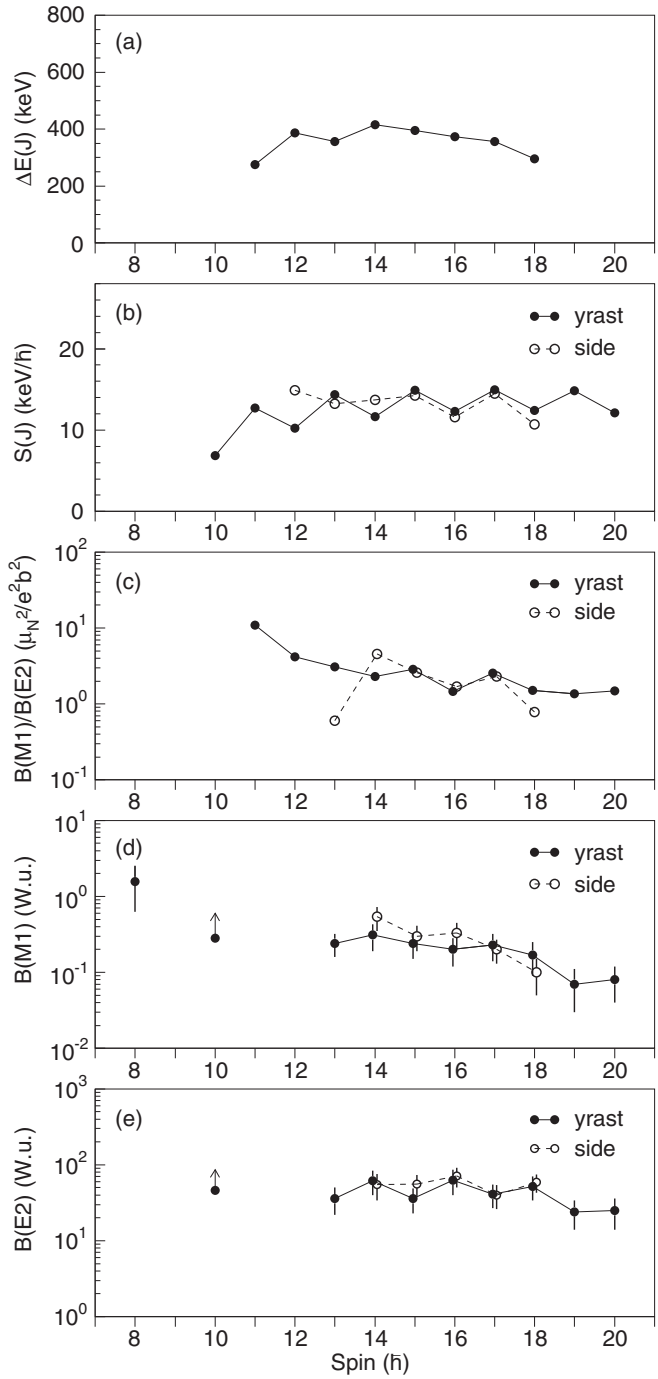

FIG. 6. Values of the energy separation $\Delta E(J)$ (a), staggering $S(J)$ (b), $B(M1)/B(E2)$ ratio (c), reduced transition probability $B(M1)$ (d), and reduced transition probability $B(E2)$ (e), as a function of spin for the chiral candidate doublet bands in ^{130}La.

the 42.3-keV transition deexciting the 9^+ state in ^{130}La, a lifetime around 20 ps is calculated, significantly shorter than the lifetime of the 8^+ state.

The experimental properties of the yrast and side bands, including the presently derived in-band $B(M1)$ and $B(E2)$ values, are illustrated in Fig. 6 and discussed in comparison with the requirement for a chiral description.

The energy separation between the bands, $\Delta E(J) = E_{\rm side}(J) - E_{\rm yrast}(J)$, is nearly constant within the spin range $J = 11$–18, with an average value of 357 keV [see Fig. 6(a)]. This is somewhat smaller than the approximate value of 400 keV observed for bands in ^{132}La, but larger than the approximate value of 200 keV observed for bands in ^{126,128}Cs. Nearly constant energy separation reflects the similar moments of inertia of the two bands.

A consequence of chiral geometry is manifested in the constancy of the energy staggering parameter $S(J)$, defined as $S(J) = [E(J) - E(J-1)]/2J$, as a function of spin. Qualitatively, this can be understood by the fact that the angular momenta of the odd particles are both perpendicular to the rotation axis and thus are not affected by the rotation, As discussed in Ref. [12], the chiral geometry is expected to arise above a critical frequency. Therefore one should observe strong energy staggering below this frequency, and a constancy of $S(J)$ as a function of spin above it. In panel (b) of Fig. 6 the energy staggering values are shown for the yrast and side bands in ^{130}La. The yrast band exhibits a strong energy staggering over the whole spin range, and some staggering is present also at higher spins of the side band. Moreover they show signature inversion, with the even-spin levels of the band favored energetically, while in the case of normal signature splitting the odd-spin members should be favored. It is worthwhile to mention that the low-spin signature is inverted for all observed yrast $\pi h_{11/2} \otimes \nu h^{-1}_{11/2}$ bands of odd-odd Cs, La, Pr, Pm, and Eu nuclei around $A \approx 130$ [42]. In some isotopes of the region a transition from the abnormal signature to the normal one has been observed at higher spins. However, this does not happen in the case of ^{130}La, where the $S(J)$ values show signature inversion over the whole spin range.

The energy staggering of the $\pi h_{11/2} \otimes \nu h^{-1}_{11/2}$ band in the odd-odd $^{124\text{–}130}$Cs nuclei was recently discussed in Ref. [43]. These nuclei are considered good examples for chirality based on electromagnetic moment measurements. The analysis revealed that in ^{124,126,130}Cs the energy staggering is present below a spin value J around 14, then up to spin around 20 it disappears or is suppressed. However in ^{128}Cs the expected constancy of $S(J)$ in the region of chirality seems to be not confirmed. As seen in Fig. 3 of Ref. [43], in this case the staggering is visible over the whole spin range, similar to the case of ^{130}La.

The $B(M1; J \to J-1)/B(E2; J \to J-2)$ values determined by using transition energies and branching ratios in the yrast band show a smooth decreasing trend up to spin 14, while an odd-even spin dependence is observed for spin values between 15 and 18 [Fig. 6(c)]. In this spin range also the $B(M1; J \to J-1)/B(E2; J \to J-2)$ values in the side band exhibit an odd-even spin dependence. However, this is not due to a staggering in $B(M1)$ values, as they show for both bands a nearly monotonic decrease with increasing spin [see Fig. 6(d)]. An interesting feature revealed by our data is an odd-even spin dependence in the $B(E2)$ values [panel (e) of Fig. 6]. We deduced therefore that the observed staggering of $B(M1)/B(E2)$ values is caused by the staggering in the $B(E2)$ values. It is interesting to mention that a staggering of

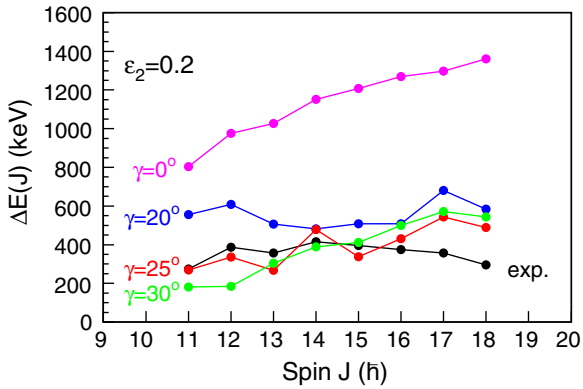

FIG. 7. Comparison of the experimental energy separation with calculated values at different γ deformations.

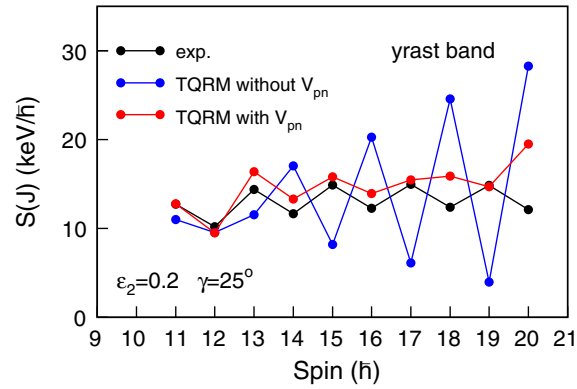

FIG. 8. Experimental signature splitting compared with calculation using the two-quasiparticle-plus-triaxial-rotor model, without and with the residual proton-neutron interaction.

the experimental $B(E2)$ values was previously reported on the basis of lifetime measurements for the yrast bands in ^{103,104}Rh nuclei [44]. Note that a weak odd-even spin staggering of $B(E2)$ transition strengths is visible also within the yrast band of ^{126}Cs [43].

In order to describe the properties of the doublet bands in ^{130}La, we performed calculations using the two-quasiparticles-plus-rotor model (TQRM) code of Ref. [45]. The model Hamiltonian includes the rotational energy of the core (which can be either axially symmetric or triaxial) and the quasiparticle energies of the odd proton and neutron. All proton and neutron orbitals originating from the $h_{11/2}$ subshell were included. The single-particle potential we used was of the modified oscillator type, with the κ and μ parameters taken from Ref. [46]. The pairing gap and the Fermi levels were derived from a BCS treatment of pairing. The interaction strengths were obtained by multiplying 0.95 to the standard strengths [47] in order to take into account the blocking effect. The core moments of inertia were calculated in such a way that the experimental energy of the 2^+ state of the even-even ^{128}Ba nucleus was reproduced. In evaluation of the electromagnetic moments, an effective g_s factor of $0.7g_s^{\text{free}}$ was used and g_R was taken as Z/A. Quadrupole moments of the core were calculated macroscopically. No Coriolis attenuation factor was introduced. Calculations were performed either without an effective residual proton-neutron (p-n) interaction or by using a zero-range interaction $V_{pn} = \sqrt{8\pi^3}(\hbar/m\omega)^{3/2}\delta(\mathbf{r_p} - \mathbf{r_n})(u_0 + u_1\sigma_\mathbf{p}\sigma_\mathbf{n})$ with parameters $u_0 = -7.2$ MeV and $u_1 = -0.8$ MeV, as proposed in [45] for the $A \approx 130$ mass region. A value of $\epsilon_2 = 0.20$ was used for the quadrupole deformation parameter, as predicted for the ^{130}La ground state in the macroscopic-microscopic calculations tabulated in Ref. [48]. Various values for the triaxial parameter γ between 0° and 30° were employed.

The experimental energy separation $\Delta E(J)$ is compared in Fig. 7 with calculations using $\epsilon_2 = 0.20$ and different γ deformations. For axial symmetry the side band is calculated very high in energy, at around 800 keV at spin 11, up to around 1400 keV at spin 18. To reproduce the experimental values, the inclusion of triaxiality is essential. We found that the best description of experimental energy separation is obtained for $\gamma = 25°$.

The use of the residual proton-neutron interaction was crucial for describing the observed signature inversion at low spins of the yrast band. Figure 8 illustrates the comparison between the experimental data with TQRM calculations performed either without V_{pn} interaction or with this interaction included. Without the residual interaction a large normal signature splitting is calculated starting from spin $J = 13$, in total disagreement with the experimental data. On the other hand, the inclusion of V_{pn} interaction nicely reproduced the inverted splitting from spin 11. The splitting is calculated to decrease with increasing spin and almost disappears between spins 15 and 19, in accordance with the predictions for chiral geometry. This is not supported by the experimental data.

The experimental reduced transition probabilities $B(M1, J \to J-1)$ and $B(E2, J \to J-2)$ for in-band transitions in the yrast and side bands, as well as the interband $B(M1, J \to J-1)$ transitions, are compared in Fig. 9 with the TQRM calculations. For the spin range 13–20 the calculations predict a strong odd-even spin dependence of the $B(M1)$ values. The $B(M1)$ values for $\Delta J = 1$ transitions connecting the side to yrast band should have odd-even staggering opposite in phase with respect to the staggering for in-band $M1$ transitions. A smooth increase with decreasing spin below spin 12 is seen in the calculated $B(M1)$ strengths of the yrast band. Note that the $B(M1)$ value derived in the present experiment for spin 8 is nicely reproduced by the TQRM calculations. However, the predicted staggering of in-band values is not confirmed by the experimental data, which show a nearly monotonic spin dependence. Moreover the interband transition probabilities are much weaker than the calculated values.

The calculated $B(E2)$ values show a smooth increase with spin. Note that an increasing behavior in the rotational $B(E2)$ values, attributed to the fixed nuclear shape, has been reported for the $\pi h_{11/2} \otimes \nu h_{11/2}^{-1}$ configuration in previous particle-rotor calculations [8,11], as well as in recent angular-momentum-projection calculations [19,20]. However, the presently measured $B(E2)$ values do not show such an increase with spin, but exhibit instead a flat behavior with an

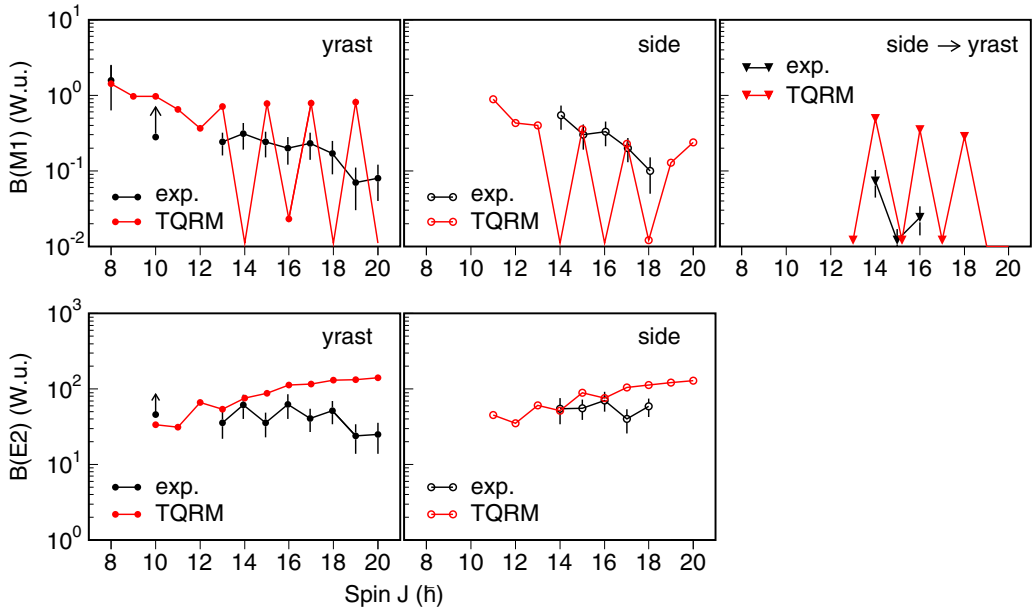

FIG. 9. Comparison of the experimental $B(M1)$ and $B(E2)$ reduced transition strengths for in-band and interband transitions (black) compared with the calculated values using the TQRM for deformation parameters $\epsilon_2 = 0.2$ and $\gamma = 25^\circ$ (red).

odd-even spin dependence. They are somewhat overestimated by the calculation even at low spins; this could indicate that the employed quadrupole deformation $\epsilon_2 = 0.2$ is too large.

Static chirality has been shown to be a transient phenomenon. The chiral motion evolves from chiral vibrations at low spins to tunneling between well-established left-handed and right-handed configurations at high spins which corresponds to static chirality [10,14,19,49]. It was shown that the $B(M1)$ staggering is weak in the chiral vibration region while it is strong in the static chirality region. In this respect an interesting case is the ^{135}Nd nucleus, in which the doublet bands described by the $\pi h_{11/2}^2 \otimes \nu h_{11/2}^{-1}$ configuration were found to exhibit similar $B(M1)$ and $B(E2)$ reduced transition probabilities and weak $B(M1)$ staggering, associated with a transition from a vibrational into a static chiral regime [49]. The present experimental data reveal that the $B(M1)$ and $B(E2)$ values for the in-band transitions of the two partner bands are essentially the same, pointing to their identical nature. However, the absence of staggering of the in-band $B(M1)$ values indicates that the static chirality is not realized. The observed electromagnetic properties could suggest a chiral vibrational regime for the doublet bands of ^{130}La. Interestingly, very different behaviors were reported for the bands based on the $\pi h_{11/2} \otimes \nu h_{11/2}^{-1}$ configuration in the neighboring ^{128}Cs and ^{132}La nuclei. Thus, the partner bands in ^{128}Cs have similar $B(M1)$ and $B(E2)$ transitions and $B(M1)$ staggering, revealing the chiral symmetry breaking phenomenon that corresponds to static chirality [23]. On the other hand the electromagnetic properties of the yrast and side bands in ^{132}La differ significantly, leading to the conclusion that they are not chiral partners [50]. It appears that the electromagnetic properties of the chiral candidate bands are extremely sensitive to nuclear structure effects such as the occupation probability of the valence quasiparticle orbitals, as well as to the details of the coupling between valence nucleons.

The orientation of the angular momentum in the intrinsic frame as a function of the spin has been studied in detail in theoretical works devoted to nuclear chirality [12,19,20,51]. It was found that at low spins the planar component with the three angular momentum vectors lying almost in one plane is dominant, while, with the increase of spin, aplanar rotation develops in both bands. A direct evidence for the planar coupling at the bandhead of the chiral rotational band in ^{128}Cs was provided very recently by its measured g factor [52]. Further experimental and theoretical investigations, including electromagnetic transition probabilities studies, are needed for understanding the complex phenomenon of chiral rotation in atomic nuclei.

V. SUMMARY

In the present study the in-band and interband reduced transition probabilities $B(M1)$ and $B(E2)$ have been deduced for the chiral-candidate doublet bands in ^{130}La on the basis of lifetime measurements performed by applying the DSAM and the fast-timing method. A lifetime of $\tau(7^+) = 0.38(7)$ ns has been derived for the 7^+ bandhead of the yrast band. The previously known side band has been extended and transition intensities within this band have been derived. Similar $B(M1)$ and $B(E2)$ values for the in-band transitions of the yrast and side bands have been obtained. The interband $M1$ transition strengths were found to be much weaker than the in-band ones. The properties of the positive-parity doublet bands in ^{130}La have been studied by using the two-quasiparticles-plus-triaxial-rotor model. The energy differences $\Delta E(J)$, the energy staggering $S(J)$, and the in-band and interband $B(M1)$

and $B(E2)$ transition strengths were calculated and compared with the experimental data. The best description of experimental energy separation was obtained for $\gamma = 25^\circ$. The observed signature inversion of the yrast band has been nicely reproduced at lower spins by including a residual proton-neutron interaction. The calculated in-band $B(M1)$ values show odd-even spin dependence in the spin range 13–20, in contrast with experimental values which slightly decrease nearly monotonically with spin. The absence of staggering in measured $B(M1)$ indicates that the static chirality regime is not realized; the chirality, if it exists, could be of vibrational type. An odd-even staggering evidenced in the $B(E2)$ values, observed also in a few other cases, is an interesting phenomenon not yet understood that requires further theoretical investigations.

ACKNOWLEDGMENTS

Authors are thankful to the FN Tandem staff of the Horia Hulubei National Institute of Physics and Nuclear Engineering for the good quality of the delivered beam. S.A. acknowledges financial support from the Scientific and Technological Research Council of Turkey (TUBTAK) BIDEB-2219 Postdoctoral Research program.

[1] S. Frauendorf and J. Meng, Nucl. Phys. A **617**, 131 (1997).
[2] V. I. Dimitrov, S. Frauendorf, and F. Dönau, Phys. Rev. Lett. **84**, 5732 (2000).
[3] K. Starosta *et al.*, Phys. Rev. Lett. **86**, 971 (2001).
[4] T. Koike, K. Starosta, C. J. Chiara, D. B. Fossan, and D. R. LaFosse, Phys. Rev. C **63**, 061304(R) (2001).
[5] B. W. Xiong and Y. Y. Wang, At. Data Nucl. Data Tables **125**, 193 (2019).
[6] J. Peng, J. Meng, and S. Q. Zhang, Phys. Rev. C **68**, 044324 (2003).
[7] T. Koike, K. Starosta, and I. Hamamoto, Phys. Rev. Lett. **93**, 172502 (2004).
[8] S. Y. Wang, S. Q. Zhang, B. Qi, and J. Meng, Phys. Rev. C **75**, 024309 (2007).
[9] S. Q. Zhang, B. Qi, S. Y. Wang, and J. Meng, Phys. Rev. C **75**, 044307 (2007).
[10] B. Qi, S. Q. Zhang, J. Meng, S. Y. Wang, and S. Frauendorf, Phys. Lett. B **675**, 175 (2009).
[11] B. Qi, S. Q. Zhang, S. Y. Wang, J. M. Yao, and J. Meng, Phys. Rev. C **79**, 041302(R) (2009).
[12] P. Olbratowski, J. Dobaczewski, J. Dudek, and W. Plóciennik, Phys. Rev. Lett. **93**, 052501 (2004).
[13] P. W. Zhao, Phys. Lett. B **773**, 1 (2017).
[14] D. Almehed, F. Dönau, and S. Frauendorf, Phys. Rev. C **83**, 054308 (2011).
[15] K. Starosta, C. J. Chiara, D. B. Fossan, T. Koike, T. T. S. Kuo, D. R. LaFosse, S. G. Rohoziński, Ch. Droste, T. Morek, and J. Srebrny, Phys. Rev. C **65**, 044328 (2002).
[16] S. Brant, D. Tonev, G. de Angelis, and A. Ventura, Phys. Rev. C **78**, 034301 (2008).
[17] H. G. Ganev, A. I. Georgieva, S. Brant, and A. Ventura, Phys. Rev. C **79**, 044322 (2009).
[18] G. H. Bhat, J. A. Sheikh, W. A. Dar, S. Jehangir, R. Palit, and P. A. Ganai, Phys. Lett. B **738**, 218 (2014).
[19] F. Q. Chen, Q. B. Chen, Y. A. Luo, J. Meng, and S. Q. Zhang, Phys. Rev. C **96**, 051303(R) (2017).
[20] M. Shimada, Y. Fujioka, S. Tagami, and Y. R. Shimizu, Phys. Rev. C **97**, 024319 (2018).
[21] T. Marchlewski *et al.*, Acta Phys. Pol. B **46**, 689 (2015).
[22] K. Selvakumar *et al.*, Phys. Rev. C **92**, 064307 (2015).
[23] E. Grodner *et al.*, Phys. Rev. Lett. **97**, 172501 (2006).
[24] E. Grodner *et al.*, Phys. Lett. B **703**, 46 (2011).
[25] W. Xiaoguang *et al.*, Plasma Sci. Technol. **14**, 526 (2012).
[26] D. Tonev *et al.*, Phys. Rev. Lett. **96**, 052501 (2006).
[27] M. Ionescu-Bujor *et al.* (unpublished).
[28] D. Bucurescu *et al.*, Nucl. Instrum. Methods Phys. Res., Sect. A **837**, 1 (2016).
[29] N. Mărginean *et al.*, Eur. Phys. J. A **46**, 329 (2010).
[30] E. S. Paul, C. W. Beausang, D. B. Fossan, R. Ma, W. F. Piel, Jr., N. Xu, and L. Hildingsson, Phys. Rev. C **36**, 1853 (1987).
[31] M. J. Godfrey, Y. He, I. Jenkins, A. Kirwan, P. J. Nolan, D. J. Thornley, S. M. Mullins, and R. Wadsworth, J. Phys. G: Nucl. Part. Phys. **15**, 487 (1989).
[32] M. Ionescu-Bujor *et al.*, Phys. Rev. C **90**, 014323 (2014).
[33] J. C. Wells and N. R. Johnson, Oak Ridge National Laboratory Report No. ORNL-6689, 1991 (unpublished), p. 44.
[34] J. F. Ziegler, *The Stopping and Range of Ions in Matter* (Pergamon, Oxford, 1980), Vols. 3 and 5.
[35] J. F. Ziegler, J. P. Biersack, and V. Littmark, *The Stopping Power and Range of Ions in Solids* (Pergamon, Oxford, 1985), Vol. 1.
[36] E. Grodner *et al.*, Eur. Phys. J. A **27**, 325 (2006).
[37] T. Kibédi, T. W. Burrows, M. B. Trzhaskovskaya, P. M. Davidson, and C. W. Nestor, Jr., Nucl. Instrum. Methods Phys. Res., Sect. A **589**, 202 (2008).
[38] S. P. Roberts, T. Ahn, K. Starosta, T. Koike, C. J. Chiara, and C. Vaman, Phys. Rev. C **67**, 057301 (2003).
[39] V. Kumar, P. Das, S. Lakshmi, P. K. Joshi, H. C. Jain, R. P. Singh, R. Kumar, S. Muralithar, and R. K. Bhowmik, Phys. Rev. C **82**, 054302 (2010).
[40] J. Timár *et al.*, Phys. Rev. C **84**, 044302 (2011).
[41] I. Kuti *et al.*, Phys. Rev. C **87**, 044323 (2013).
[42] Y. Liu, J. Lu, Y. Ma, S. Zhou, and H. Zheng, Phys. Rev. C **54**, 719 (1996).
[43] T. Marchlewski, J. Srebrny, and E. Grodner, Acta Phys. Pol. B Proc. Suppl. **11**, 89 (2018).
[44] T. Suzuki *et al.*, Phys. Rev. C **78**, 031302(R) (2008).
[45] P. B. Semmes and I. Ragnarsson, in *Proceedings of the International Conference on High Spin Physics and Gamma-soft Nuclei*, Pittsburgh, 1990 (World Scientific, Singapore, 1991), p. 500.
[46] J. Y. Zhang, N. Xu, D. B. Fossan, Y. Liang, R. Ma, and E. S. Paul, Phys. Rev. C **39**, 714 (1989).
[47] S. G. Nilsson, C. F. Tsang, A. Sobiczewski, Z. Szymański, S. Wycech, C. Gustafsson, I.-L. Lamm, P. Möller, and B. Nilsson, Nucl. Phys. A **131**, 1 (1969).
[48] P. Möller, J. R. Nix, W. D. Myers, and W. J. Swiatecki, At. Data Nucl. Data Tables **59**, 185 (1995).
[49] S. Mukhopadhyay *et al.*, Phys. Rev. Lett. **99**, 172501 (2007).
[50] E. Grodner, J. Phys.: Conf. Ser. **366**, 012022 (2012).
[51] Q. B. Chen, K. Starosta, and T. Koike, Phys. Rev. C **97**, 041303(R) (2018).
[52] E. Grodner *et al.*, Phys. Rev. Lett. **120**, 022502 (2018).